# Backbone Dynamics of Calmodulin Studied by $^{15}N$ Relaxation Using Inverse Detected Two-Dimensional NMR Spectroscopy: The Central Helix Is Flexible†

Gaetano Barbato,‡,§ Mitsuhiko Ikura,‡ Lewis E. Kay,‡ Richard W. Pastor,∥ and Ad Bax*,‡

*Laboratory of Chemical Physics, National Institute of Diabetes and Digestive and Kidney Diseases, National Institutes of Health, Bethesda, Maryland 20892, and Biophysics Laboratory, Center for Biologics Evaluation and Research, Food and Drug Administration, 8800 Rockville Pike, Bethesda, Maryland 20892*

*Received December 19, 1991; Revised Manuscript Received March 31, 1992*

ABSTRACT: The backbone dynamics of $Ca^{2+}$-saturated recombinant *Drosophila* calmodulin has been studied by $^{15}N$ longitudinal and transverse relaxation experiments, combined with $^{15}N\{^1H\}$ NOE measurements. Results indicate a high degree of mobility near the middle of the central helix of calmodulin, from residue K77 through S81, with order parameters ($S^2$) in the 0.5–0.6 range. The anisotropy observed in the motion of the two globular calmodulin domains is much smaller than expected on the basis of hydrodynamic calculations for a rigid dumbbell type structure. This indicates that, for the purposes of $^{15}N$ relaxation, the tumbling of the N-terminal (L4–K77) and C-terminal (E82–S147) lobes of calmodulin is effectively independent. A slightly shorter motional correlation time ($\tau_c \approx 6.3$ ns) is obtained for the C-terminal domain compared to the N-terminal domain ($\tau_c \approx 7.1$ ns), in agreement with the smaller size of the C-terminal domain. A high degree of mobility, with order parameters of ~0.5, is also observed in the loop that connects the first with the second EF-hand type calcium binding domain and in the loop connecting the third and fourth calcium binding domain.

Calmodulin (CaM) is a ubiquitous intracellular protein of 148 residues ($M_r$ 16.7K) that plays a key role in coupling $Ca^{2+}$ transients caused by a stimulus at the cell surface to events in the cytosol (Cohen & Klee, 1988). It performs this role by calcium-dependent binding to a host of intracellular enzymes. Its crystal structure (Babu et al., 1988) shows that the protein consists of two globular domains, each containing two calcium binding sites of the "EF-hand" type, connected by a continuous 26-residue $\alpha$-helix, often referred to as the "central helix". Consequently, in the crystalline state CaM adopts a dumbbell type structure. Small-angle X-ray scattering studies of CaM in solution (Seaton et al., 1985; Heidorn & Trewhella, 1988; Matsushima et al., 1989) agree on the presence of the two globular lobes in calmodulin, but disagree on the question of whether these lobes are separated by a large fixed distance as in the crystal structure, or by either a "flexible tether" type central helix or a bent one.

Very recently, the crystal structure for recombinant CaM from *Drosophila melanogaster* was reported (Taylor et al., 1991). Although there were some differences with the structure of bovine brain calmodulin (Babu et al., 1988), the overall shape of the two molecules is very similar. At the time the present study of the CaM dynamics was conducted, the coordinates of the recombinant protein were not yet available, and in our discussions we refer to the structure of the bovine CaM structure, although our studies are actually carried out using recombinant CaM from *Drosophila melanogaster*.

Using recently developed triple-resonance NMR techniques, we previously made complete assignments of the $^1H$, $^{13}C$, and $^{15}N$ NMR spectra of this protein and determined its secondary structure in aqueous solution (Ikura et al., 1991a,b). NOE data indicated that the so-called "central helix" is disrupted from residue Asp-78 through Ser-81. Spera et al. (1991) found that the hydrogen exchange rates of residues located near the middle of the central helix are fast, suggesting that hydrogen bonding for these amides is either weak or absent. The NOEs observed for these residues are relatively weak and do not point to a helical structure. The secondary shifts (i.e., the deviations from random coil chemical shifts) of the C$\alpha$ carbons and C$\beta$ carbons for these residues are also relatively small in this region of the protein (Ikura et al, 1991a,b). These NMR data suggest that there may be a significant degree of mobility in the protein near the middle of the central helix.

The present study measures the NMR relaxation properties of backbone $^{15}N$ nuclei in engineered calmodulin by using highly sensitive indirect detection techniques (Nirmala & Wagner, 1988; Kay et al., 1989). The relaxation data both provide unambiguous measures for the degree of internal motion of individual backbone amides and report on the anisotropy of the molecular reorientation. Our analysis largely followed similar studies conducted previously for staphylococcal nuclease (Kay et al., 1989) and interleukin-1$\beta$ (Clore et al., 1990a). However, recently improved techniques for measurement of $^{15}N$ relaxation rates, which suppress the effect of cross correlation between dipolar and chemical shift anisotropy (Boyd et al., 1990; Kay et al., 1992; Palmer et al., 1992), are used in the present study. In addition, these pulse schemes have been modified to remove the need for $H_2O$ presaturation. This permits the study of amides for which the proton exchanges rapidly with solvent, as occurs for the most mobile residues of calmodulin.

Relaxation data are analyzed using the model-free approach of Lipari and Szabo (1982), and apparent rotational correlation times are derived for the individual amides. The dependence of the measured rotational correlation time on the orientation of the N–H bond vector in a molecular axis system is used to provide information on the degree of anisotropy of the molecular tumbling. This degree of anisotropy in molecular reorientation is compared with the anisotropy evaluated from hydrodynamic calculations on a variety of slightly dif-

† This work was supported by the Intramural AIDS Anti-viral Program of the Office of the Director of the National Institutes of Health.

‡ National Institutes of Health.

§ On leave from Universita di Napoli, Federico II, Dipartimento di Chimica, Via Mezzocannone 4, 80134 Napoli, Italy.

∥ Food and Drug Administration.

ferent rigid calmodulin models.

## Materials and Methods

*Sample Preparation.* Recombinant *Drosophila* CaM was prepared with *Escherichia coli* (strain AR58) harboring the pAS expression vector (Shatzman & Rosenberg, 1985). Uniform $^{15}N$ labeling at a level of more than 95% was obtained by growing the bacteria in M9 minimal medium with [$^{15}N$]-$NH_4Cl$ (Isotec Inc.) as the sole nitrogen source. Engineered calmodulin lacks the posttranslational N-acetylation and the trimethylation of the $\epsilon$-amino group of K115. The protein was purified as described previously (Ikura et al., 1990b). A 0.4-mL sample was prepared in 95% $H_2O$/5% $D_2O$ with a 1.5 mM concentration of CaM, 6.1 mM $CaCl_2$, and 100 mM KCl, pH 6.3. Transverse relaxation time measurements made on a 0.7 mM CaM sample yielded an increase in $T_2$ by $\sim 6 \pm 2\%$ relative to the 1.5 mM solution, suggesting that this relaxation time (and the rotational diffusion rate) does not increase by more than $\sim 10\%$ upon infinite dilution.

*NMR Spectroscopy.* $^{15}N$ $T_1$ and $T_2$ measurements were carried out at 35 °C on a Bruker AM-500 spectrometer operating at 500-MHz $^1H$ frequency. $^{15}N\{^1H\}$ NOEs were measured both on the AM-500 spectrometer and at 600-MHz $^1H$ frequency on a Bruker AMX-600 spectrometer. The pulse schemes used in the present study are illustrated in Figure 1. The schemes for $T_1$ and $T_2$ measurement are identical to the schemes recently described by Kay et al. (1992) and Palmer et al. (1992), apart from the inclusion of "scrambling pulses" (Messerle et al., 1989) which remove the need for presaturation of the $H_2O$ resonance.

$^{15}N$ $T_1$ measurements were conducted with the pulse scheme of Figure 1a. 32 scans were acquired for each $t_1$ increment; quadrature in the $F_1$ dimension was obtained using time-proportional phase incrementation (TPPI). The $^1H$ carrier was positioned at 8.65 ppm and the $^{15}N$ carrier at 118 ppm. The spectral widths used were 8.0 ppm ($^1H$, $F_2$) and 30.0 ppm ($^{15}N$, $F_1$). A 512 × 1024 real data matrix was acquired for six different durations of the $T_1$ relaxation delay, $T$ = 26, 82, 138, 306, 502, and 853 ms. A 1.2-s relaxation delay was used between scans. $T_2$ measurements, conducted with the scheme of Figure 1b, were recorded with the same spectral widths, number of scans, and data matrix sizes as the $T_1$ data, but with six different $T_2$ relaxation delays of 8.7, 22, 43, 70, 104, and 156 ms. Note that both the $T_1$ and $T_2$ experiments are performed in such a way that the signal decays to zero for long relaxation delays, allowing a two-parameter fit of the magnetization decay curves and making the measurement independent of the delay time between scans (Sklenar et al., 1987).

The $^{15}N\{^1H\}$ NOE was measured with the scheme of Figure 1c. For quantitative measurement of the NOE it is essential to record two spectra, one with the NOE effect, and one without. The $^1H$ carrier was positioned on the $H_2O$ resonance and a 400 × 1024 real data matrix was acquired, using acquisition times of 132 ms ($t_1$) and 51 ms ($t_2$). The spectrum with NOE was obtained by using the pulse scheme of Figure 1c preceded by $H_2O$ presaturation between scans, and in addition, nonselective 120° pulses (with the same RF phase as the $H_2O$ presaturating field) were applied every 20 ms, thus ensuring that the protons remained in a saturated state. The spectrum without NOE was recorded with identical parameters, except for the absence of $H_2O$ presaturation and the 120° pulses. Instead, to suppress the strong $H_2O$ resonance, two high-power 10-ms scrambling pulses of identical RF phase, separated by a 1-ms delay, were applied immediately prior to the first 90° ($^{15}N$) pulse, with the $^1H$ carrier positioned on the

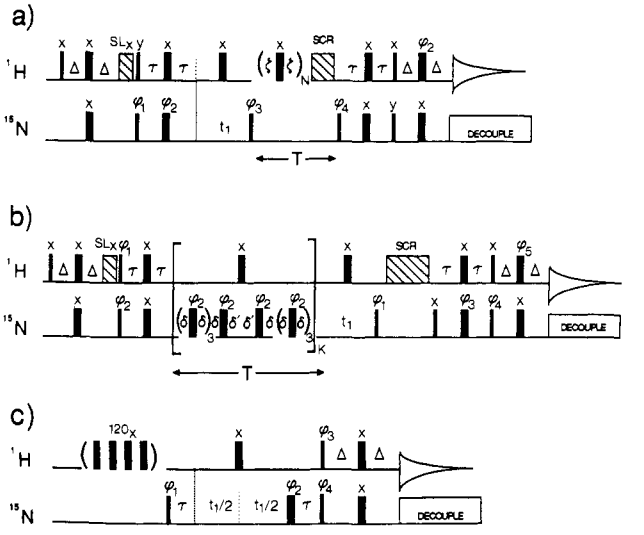


FIGURE 1: Pulse sequences used for the measurement of $^{15}N$ (a) $T_1$ and (b) $T_2$ relaxation times, and (c) for measurement of the $^{15}N\{^1H\}$ NOE. The pulse sequences are similar to those reported by Kay et al. (1992) apart from the absence of $H_2O$ presaturation and the introduction of spin lock (SL) (Messerle et al., 1989) and scrambling (SCR) pulses used to dephase $H_2O$ magnetization. The spin lock pulses are applied at high power and have a duration of 1 ms. The scrambling pulses are also applied at high power and have a duration of 12 ms. For sequences a and b, the $^1H$ carrier was positioned in the center of the amide region and temporarily jumped to the $H_2O$ frequency for application of the scrambling pulses. For (c) the carrier was positioned at the $H_2O$ frequency throughout. For (c), the 120° high-power pulses are applied during the entire delay between scans (3 s) at 20-ms intervals, to maintain a saturated state of the $^1H$ reservior. For obtaining the reference spectrum without NOE, the 120° pulses were omitted and, instead, two scrambling pulses of 10 ms each, spaced by 1 ms, were introduced immediately prior to the 90°$_{\phi_1}$ $^{15}N$ pulse in order to eliminate the $H_2O$ signal. In sequences a and b, the effects of cross correlation between $^{15}N$–$^1H$ dipolar coupling and $^{15}N$ chemical shift anisotropy are eliminated by periodic application of 180° $^1H$ pulses during the $T_1/T_2$ relaxation period of duration $T$. Delay durations used are as follows: $\Delta$ = 2.25 ms; $\tau$ = 2.75 ms; $\zeta$ = 7 ms; $\delta$ = 0.45 ms; $\delta' = \delta - \tau_{90}(^1H)$, where $\tau_{90}(^1H)$ is the duration of a $^1H$ 90° pulse (11 $\mu$s). To increment the relaxation delay, $T$, the loop counters $N$ (for scheme a) and $K$ (for scheme b) are incremented. The phase cycling used is as follows: for scheme a, $\phi_1 = 4(x), 4(-x)$; $\phi_2 = 8(x), 8(y), 8(-x), 8(-y)$; $\phi_3 = y, -y$; $\phi_4 = 2(x), 2(-x)$; Acq = $x, 2(-x), x, -x, 2(x), -x$. For scheme b, $\phi_1 = y, -y$; $\phi_2 = 2(x), 2(-x)$; $\phi_3 = 16(x), 16(-x)$; $\phi_4 = 8(y), 8(-y)$; $\phi_5 = 4(x), 4(y)$; Acq = $2(x), 4(-x), 2(x), 2(-x), 4(x), 2(-x)$. For scheme c, $\phi_1 = x, -x$; $\phi_2 = 8(x), 8(y), 8(-x), 8(-y)$; $\phi_3 = 2(x), 2(-x)$; $\phi_4 = 4(y), 4(-y)$; Acq = $x, 2(-x), x, -x, 2(x), 2(-x), 2(x), -x, x, 2(-x), x$.

$H_2O$ frequency. In principle, the fact that the protons are in a saturated state 21 ms prior to measurement gives rise to a small truncated NOE effect. However, considering that the $^1H$–$^{15}N$ cross relaxation times are much longer than 21 ms, this effect may safely be neglected. The sensitivity of the NOE measurement is significantly lower compared to the $T_1$ and $T_2$ measurements, mainly because no $^1H \rightarrow {}^{15}N$ polarization transfer step is used in the NOE experiment. In addition, a relatively long delay between scans [$>3T_1(^{15}N)$ and $>3T_1(^1H)$] must be used (3 s in our experiments) to ensure that the $^{15}N$ magnetization has reached its equilibrium value prior to the first 90°($^{15}N$) pulse. The experiment was repeated with slightly higher sensitivity at 600 MHz, on an AMX-600 spectrometer, using similar conditions.

The $T_1$, $T_2$, and NOE data sets were processed using Lorentzian-to-Gaussian filtering functions in both dimensions, and zero filling to 2048 and 4096 data points was used in the $t_1$ and $t_2$ dimension, respectively. The processing and peak picking were carried out using the software package NMR2

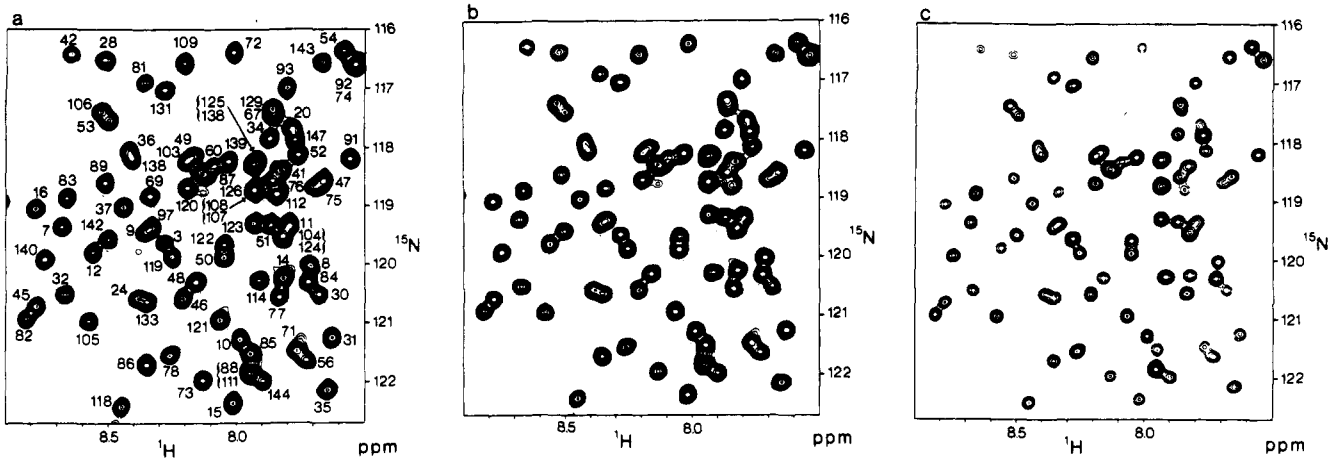


FIGURE 2: Contour plots of the most crowded region of the $^1H$–$^{15}N$ shift correlation spectrum recorded with the $T_2$ scheme of Figure 1b, using relaxation delays, $T$, equal to (a) 8.7 ms, (b) 43 ms, and (c) 156 ms.

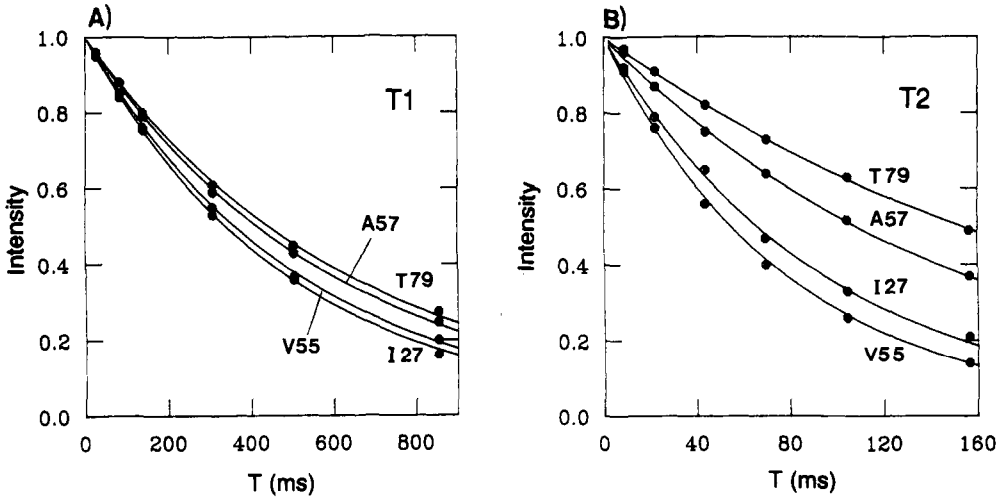


FIGURE 3: (A) $T_1$ and (B) $T_2$ decay curves for four amino acids with substantially different relaxation rates. Drawn curves represent calculated least-squares best fits to single exponential decays.

(NMRi, Syracuse, NY). Resonance intensities rather than integrated peak volumes were used to determine relaxation rates because accurate integration requires well-separated resonances. Note that the line shape of an individual resonance is independent of the relaxation delay, $T$. Therefore, integration and peak intensity give identical results for the relaxation times of well-resolved resonances, as confirmed experimentally.

## Results and Analysis

*$T_1$, $T_2$, and NOE Relaxation Data.* The three panels of Figure 2 show the most crowded region of the $^{15}N$–$^1H$ shift correlation spectrum, recorded with the pulse scheme of Figure 1b, for three different values of the transverse relaxation delay. Representative $T_1$ and $T_2$ magnetization decay curves for a number of residues with significantly different relaxation rates are shown in Figure 3. The relaxation rates were determined by best fitting of the decay curves to a single exponential, using conjugate gradient methods. The average standard error was 1.8% for fitting the $T_2$ data and 2.3% for the $T_1$ data.

Assessment of the error in the NOE data is more complicated than for the $T_1$ and $T_2$ measurements. Comparison of the NOE data recorded for 37 homologous residues in the N- and C-terminal domains of calmodulin (excluding Lys-115) after correcting for the difference in the average value ($\langle NOE_N \rangle = \langle NOE_C \rangle + 0.04$) gives a root-mean-square difference of 0.07. This suggests a standard error of 0.05, assuming that the errors in the N- and C-terminal domains are uncorrelated and of the same magnitude. Comparison of the NOE data recorded at 500 and 600 MHz shows, as theory predicts, that the 600-MHz NOE on average is higher than the 500-MHz NOE ($\langle NOE_{600} \rangle = \langle NOE_{500} \rangle + 0.04$). With the exception of a few residues, for which a 500-MHz NOE higher than the theoretical limit was measured, the 600-MHz NOE never was more than 0.08 lower than the 500-MHz one; the smaller of the two NOEs is reported in Table S1 and used in our calculations. The measured $T_1$, $T_2$, and NOE data are reported in supplementary Table S1 for 114 (77%) of the residues in calmodulin for which a resolved $^1H$–$^{15}N$ correlation is observed. The data are also summarized in panels a, b, and c of Figure 4.

*Analysis of $T_1$, $T_2$, and NOE Data.* Analysis of the $T_1$, $T_2$, and NOE data follows the procedure outlined by Kay et al. (1989) and Clore et al. (1990a). Equations relating the $T_1$, $T_2$, and NOE enhancements of an amide $^{15}N$ spin in the presence of heteronuclear dipolar coupling and chemical shift anisotropy used in the present work are identical to eq 1–3 of Kay et al. (1989) and will not be repeated here.

The relaxation data are analyzed using the "model-free" approach of Lipari and Szabo (1982). They postulate the correlation function for internal motions to be given by

$$C_I(t) = S^2 + (1 - S^2) \exp(-t/\tau_e) \quad (1)$$

where $S^2$ is a generalized order parameter, measuring the

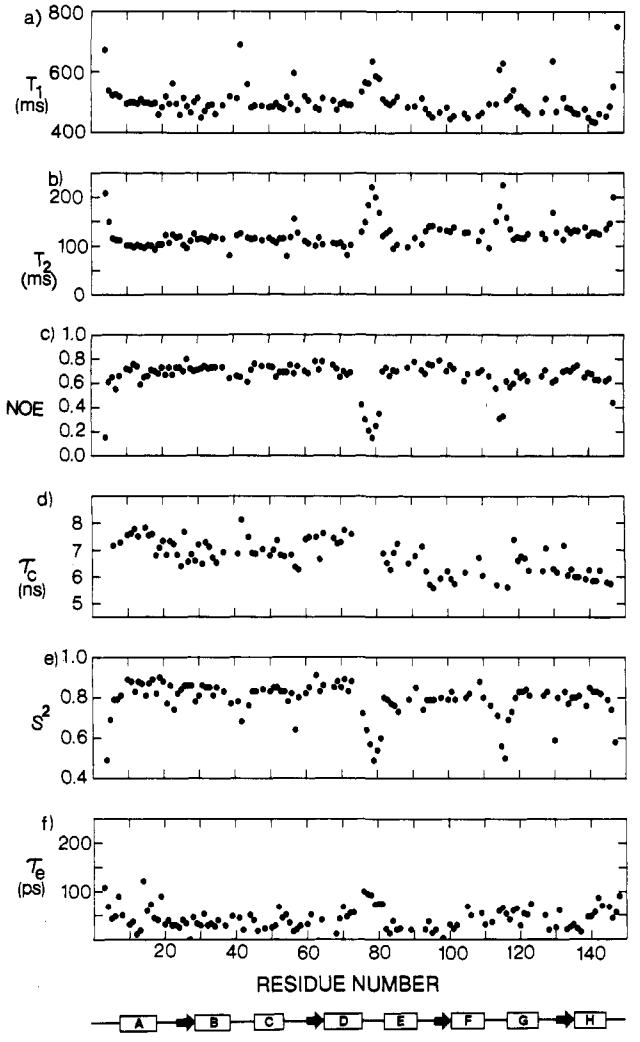


FIGURE 4: Plots as a function of residue number of (a) the measured $T_1$ and (b) $T_2$ values, (c) the $^{15}N\{^1H\}$ NOE, (d) the rotational correlation time derived from $T_1/T_2$, (e) the order parameter, $S^2$, and (f) the value for the correlation time of internal motion, $\tau_e$. Only residues for which the $^{15}N$–$^1H$ correlation is sufficiently well resolved to permit accurate measurement of its intensity are included. $\tau_c$ values are not calculated for residues with anomolously short $T_2$ values (cf. eq 7) and for residues with a significant NOE contribution (NOE < 0.6).

degree of spatial restriction of (rapid) internal motions of the N–H bond vector, and $\tau_e$ is the effective correlation time of these rapid local fluctuations. For a spherical molecule with overall rotational correlation time $\tau_c$, this gives rise to a spectral density function of the form:

$$J(\omega) = S^2\tau_c/[1 + (\omega\tau_c)^2] + (1 - S^2)\tau/[1+ (\omega\tau)^2] \quad (2)$$

where $1/\tau = 1/\tau_c + 1/\tau_e$.

For an axially symmetric molecule, with different rotational diffusion coefficients parallel ($D_\parallel$) and perpendicular ($D_\perp$) to the unique axis of the molecule, one obtains a more complex spectral density function approximated by (Woessner, 1960; Huntress, 1968; Hubbard, 1970)

$$J(\omega) = S^2\{A_1\tau_1/[1 + (\omega\tau_1)^2] + A_2\tau_2/[1 + (\omega\tau_2)^2] + A_3\tau_3/[1 + (\omega\tau_3)^2]\} + (1 - S^2)\tau/[1 + (\omega\tau)^2] \quad (3)$$

with

$$A_1 = 0.75 \sin^4 \alpha \quad (4a)$$

$$A_2 = 3 \sin^2 \alpha \cos^2 \alpha \quad (4b)$$

$$A_3 = (1.5 \cos^2 \alpha - 0.5)^2 \quad (4c)$$

where $\alpha$ is the angle between the N–H bond vector and the cylinder axis. The correlation times $\tau_1$, $\tau_2$, and $\tau_3$ depend on the rotational diffusion rates in the following manner:

$$\tau_1 = (4D_\parallel + 2D_\perp)^{-1} \quad (5a)$$

$$\tau_2 = (D_\parallel + 5D_\perp)^{-1} \quad (5b)$$

$$\tau_3 = (6D_\perp)^{-1} \quad (5c)$$

As in eq 2, $\tau$ in eq 3 is dominated by the time constant describing fast internal motions but also depends on that of the (anisotropic) overall motion. When the internal motion is at least 1 order of magnitude faster than any of the three correlation times, $\tau_1$, $\tau_2$, and $\tau_3$, we assume

$$1/\tau = 1/\tau_e + 1/\tau_{c,eff} \quad (6a)$$

with

$$\tau_{c,eff} = 1/6D_{eff} = (4D_\perp + 2D_\parallel)^{-1} \quad (6b)$$

where $D_{eff}$ is approximated by one-third of the trace of the diffusion tensor.

*Determination of the Rotational Correlation Time.* For axially symmetric anisotropic tumbling, the $T_1$ and $T_2$ relaxation times are functions of three different correlation times for molecular reorientation (eq 5), as well as the correlation time $\tau_e$ for internal fluctuations. Without extensive field dependence studies of the $^{15}N$ relaxation behavior, it is not possible to derive these four individual correlation times, $\tau_1$, $\tau_2$, $\tau_3$, and $\tau_e$, separately for each of the backbone $^{15}N$ nuclei. Therefore, first we analyze our data as if there were no anisotropy of motion and derive apparent rotational correlation times, $\tau_c$, in a manner previously described by Kay et al. (1989) and Clore et al. (1990a). In the Appendix we report what such an analysis is expected to yield for a protein with an anisotropic diffusion tensor.

As discussed previously (Kay et al., 1989; Clore et al., 1990a), the effect of rapid motions (on the time scale $\tau_e$) may be ignored for calculating an effective correlation time, $\tau_c$, because to a first approximation these rapid motions lengthen both the $T_1$ and $T_2$ values by the same fraction. This makes it possible to calculate $\tau_c$ from the $T_1/T_2$ ratio provided proper precautions are taken. First, residues that have a significant NOE effect, i.e., NOE < 0.6, are excluded because for these residues the assumption that motion on the $\tau_e$ time scale does not contribute to $T_1$ relaxation is not valid. Second, conformational averaging on a time scale which is not extremely fast compared to the difference in $^{15}N$ chemical shifts of the conformers involved can give rise to a shortening of the $T_2$ value. For a nearly spherical protein these residues can be identified by comparing the $T_1/T_2$ ratio observed for a given $^{15}N$ nucleus with the average $T_1/T_2$ ratio, and by excluding residues that fall outside the standard deviation (Clore et al., 1990a). In the present case, where the degree of motional anisotropy is the subject of interest, such a procedure cannot be followed. However, these residues can still be identified since any deviation from the average $T_1/T_2$ ratio caused by motional anisotropy must affect the measured $T_1$ and $T_2$ value in opposite ways. Therefore, residues for which the $^{15}N$ $T_2$ is affected by conformational averaging are easily recognized by a shorter $T_2$ *without* a concomitant increase in $T_1$. Consequently, a $T_2$ value of residue $n$ is excluded from the calculation if its $T_2$ exceeds the average $T_2$ value (averaged over all backbone amides present in the same domain as residue $n$ that have NOE > 0.6) by one standard deviation (SD), unless there is a significant lengthening of the $T_1$ of residue

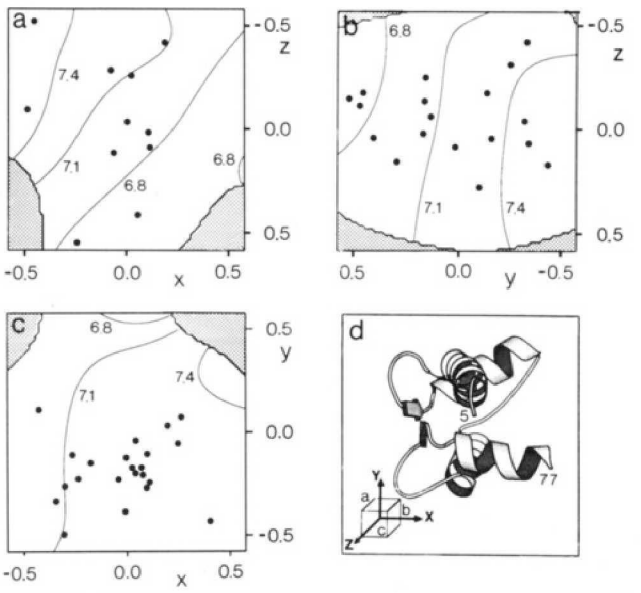


FIGURE 5: Contour plot of the distribution of rotational correlation times, $\tau_c$, as a function of the orientation of the N–H bond vector in the coordinate frame shown in panel d, for the N-terminal half of the X-ray crystal structure of calmodulin (Babu et al., 1988). Dots correspond to the position where an N–H bond vector for which a $\tau_c$ has been derived would cut through the surface of a cube that has the $^{15}$N nucleus at its center. Panels a, b, and c correspond to the *xz*, *yz*, and *xy* surfaces of the cube, respectively. Thus, for example, amides in the central helix, which have their N–H bond vectors aligned roughly parallel to the *x* axis, appear in the *yz* plane. The size of the cube has been chosen to just fit within a sphere of unit radius, i.e., the corner points of the cube are at coordinates $(x,y,x) = (\pm 0.577, \pm 0.577, \pm 0.577)$. Therefore, a dot at coordinates $(x_1,y_1)$ on the surface of the cube in the *xy* plane corresponds to an amide with its bond vector in the $(x_1,y_1,0.577)$ direction. The $\tau_c$ values have been smoothed in a manner described in the text, in order to allow a contour plot of the $\tau_c$ value as a function of orientation of the N–H bond vector. Contours are drawn at $\tau_c = 5 + N \times 0.3$ ns ($N = 0, 1, 2, \ldots$). Shaded areas correspond to regions where no contours could be calculated because of an insufficient number of N–H bond vectors pointing in these directions. The *x* axis has been chosen arbitrarily to be parallel to the average N–H bond vector orientation in the central helix (F65–F92).

*n*. Thus, a $T_2$ value measured for residue *n* is excluded from all calculations if both of the following conditions apply:

$$T_{2,n} < \langle T_2 \rangle - \mathrm{SD} \qquad (7a)$$

and

$$(T_{2,n} - \langle T_2 \rangle)/T_{2,n} > 3(\langle T_1 \rangle - T_{1,n})/T_{1,n} \qquad (7b)$$

In the N-terminal domain, the average relaxation times for residues with NOE > 0.6 are $\langle T_1 \rangle = 503 \pm 36$ ms and $\langle T_2 \rangle = 110 \pm 13$ ms, and for the C-terminal domain, $\langle T_1 \rangle = 482 \pm 34$ ms and $\langle T_2 \rangle = 125 \pm 15$ ms.

As was previously shown for staphylococcal nuclease (Kay et al., 1989) and for interleukin-1$\beta$ (Clore et al., 1990a), and as will be shown below for calmodulin, residues in regions of regular secondary structure with $^{15}$N{$^1$H} NOEs larger than ~0.7 have uniform order parameters of ~0.85. Thus, for residues with an $^{15}$N $T_2$ that is shortened by conformational exchange, an effective correlation time, $\tau_c$, often can be derived from the $T_1$ data alone. A $\tau_c$ value was calculated in this manner for all six residues that have an anomalously short $T_2$ value: L18, T27, I85, R86, F89, and D93. For all other residues with NOE > 0.6, $\tau_c$ is calculated from the $T_1/T_2$ ratio. The $\tau_c$ values obtained in this manner are given in the supplementary material (Table S1) and are displayed graphically in Figure 4d. As can be seen from this figure, the effective

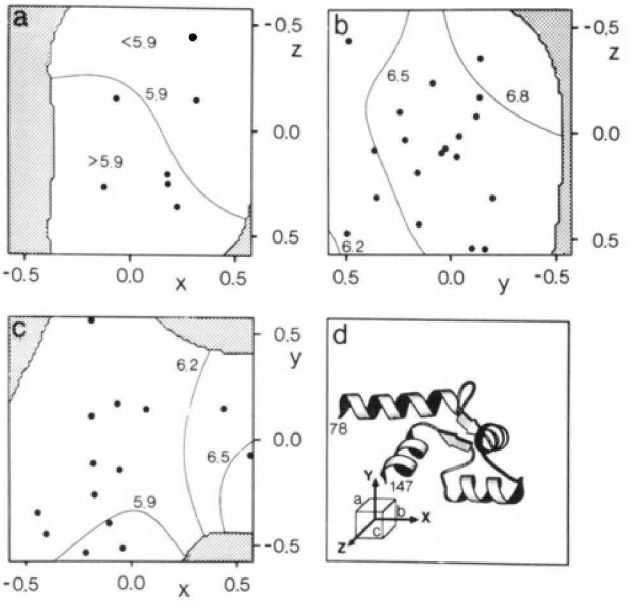


FIGURE 6: Contour plot of the average value of the rotational correlation time, $\tau_c$, as a function of the orientation of the N–H bond vector for amides in the C-terminal domain of calmodulin. The figure has been derived in the same manner as described in the legend to Figure 5.

correlation times derived in this manner for the individual backbone amides are quite uniform, with an average value of $7.12 \pm 0.42$ ns ($N = 51$) for the N-terminal domain and $6.30 \pm 0.48$ ns ($N = 40$) for the C-terminal domain, where *N* is the number of residues used for calculating the average $\tau_c$ value. The fact that the average $\tau_c$ is shorter for the C-terminal domain is not surprising considering that the number of structured residues for this half (from E82 to S147) is eight smaller compared to the structured region of the N-terminal half (L4–K77).

The small spread in the measured $\tau_c$ values suggests that there is little anisotropy in the rotational reorientation of the individual protein domains. Hydrodynamic calculations by Small and Anderson (1988) suggested that even for a rigid central helix the anisotropy of molecular reorientation would be quite small. However, as is discussed in the Appendix, their calculations were based on a simplified hydrodynamic model. Our calculations using more sophisticated hydrodynamic modeling show unequivocally that all realistic hydrodynamic models for rigid calmodulin give rise to a degree of anisotropy in molecular reorientation that is much larger than observed experimentally, indicating that calmodulin does not tumble as a rigid dumbbell.

*Observed Anisotropy of Molecular Motion.* Because NMR relaxation of an $^{15}$N nucleus is not influenced by rotation around the N–H bond vector, but only by rotations that result in the change of the direction of the N–H bond vector, anisotropy of the motion affects the spectral density function of eq 3 in a manner that depends on the orientation of the N–H bond vector relative to the axes of the molecular rotational diffusion tensor (Woessner, 1960; Huntress, 1968; Hubbard, 1970). If, however, $\tau_c$ is found to be independent of the orientation of the N–H bond vector and a sufficiently large distribution of N–H bond vectors with different orientations is available, the motion is effectively isotropic. In the following analysis we assume the N–H bond vector orientations within each globular domain to be those of the crystal structure (Babu et al., 1988). NMR studies indicate that the solution structure of the individual domains is very similar to the crystal structure (Seeholzer & Wand, 1988; Ikura et al., 1991b).

The low degree of motional anisotropy of the individual N- and C-terminal halves of calmodulin is illustrated most unambiguously in Figures 5 and 6, which show contour plots of the $\tau_c$ values (taken from the supplementary material, Table S1) as a function of the orientation of the N–H bond vector. Ideally, such contour plots would be drawn on the surface of a sphere of unit radius. However, because of the difficulty of displaying a spherical contour plot in two dimensions, we have calculated its projection on a cube. First we will briefly describe how these contour plots are derived.

The orientation of the N–H bond of amide $i$ is described by a unit vector $(x_i',y_i',z_i')$. If the absolute value of the $z_i'$ coordinate is larger than that of either $x_i'$ or $y_i'$, this vector will intersect with the front $(xy)$ surface of the cube that falls just inside the unit sphere (i.e., the diagonal length of the cube is 2). This surface is labeled "c" in the inset in Figure 5d, and the actual points where vectors intersect with this plane are marked by dots in Figure 5c. Because the N–H bond vectors in an $\alpha$-helix are approximately parallel to the helix axis, it can be seen from Figure 5d that most of the vectors that intersect with plane "c" correspond to amides in the first and third helices of the N-terminal domain. The $(x_i',y_i',z_i')$ vector intersects the $z = 0.577$ plane at $x = 0.577x'/z'$ and $y = 0.577y'/z'$. A smoothing function, $f(x,y)$ that describes the average $\tau_c$ value for a given orientation $(x,y,0.577)$ of the N–H bond vector is then calculated by convolution with a Gaussian function in the following manner:

$$f(x,y) = \sum_i \tau_{c,i} g_i(x',y',z') / \sum_i g_i(x',y',z') \quad (8)$$

where the summation extends over all residues $i$ for which a $\tau_c$ value has been calculated and $g_i(x',y',z')$ is a Gaussian weighting function of the form:

$$g_i(x',y',z') = 1/z_i' \exp[\{-(x'' - x_i'')^2 - (y'' - y_i'')^2/z_i'\}/(\text{rad})^2] \quad (9)$$

with

$$x_i'' = x_i' \cos\alpha + y_i' \sin\alpha \quad (10a)$$

$$y_i'' = -x_i' \sin\alpha + y_i' \cos\alpha \quad (10b)$$

$$x'' = x' \cos\alpha + y' \sin\alpha \quad (10c)$$

$$y'' = -x' \sin\alpha + y' \cos\alpha \quad (10d)$$

$$\cos\alpha = x_i'/r \quad (10e)$$

$$\sin\alpha = y_i'/r \quad (10f)$$

$$r = \sqrt{x_i'^2 + y_i'^2} \quad (10g)$$

The parameter "rad" determines the width of the Gaussian weighting function and has been set to 0.35 for making the figure. Shaded regions of the plot correspond to areas where the "density function" $g(x,y,z)$ is smaller than 1. The $zx$ plane (containing amides with $|y_i'| > |z_i'|, |x_i'|$), shown in Figure 5a, and the $zy$ plane (Figure 5b) are calculated in a similar manner.

As can be seen in Figure 5, although the variation in the magnitude of $\tau_c$ as a function of the orientation of the N–H bond vector is small, the longest values for $\tau_c$ (~7.5 ns) are found in panel b, corresponding to an $x$ coordinate of 0.577, at $y$ and $z$ coordinates of −0.5 and 0.2, respectively. This means that the longest $\tau_c$ values are obtained for N–H bond vectors approximately parallel to the (0.577,−0.5,0.2) vector. This vector is almost parallel to a line that connects the C$\alpha$ carbon of Met-76 (the last ordered residue of the N-terminal domain) with the center of gravity of the N-terminal domain ($\alpha = 22°$). The degree of anisotropy in $\tau_c$ is very small, however, on the order of 10–15%. A similar degree of anisotropy is observed for the C-terminal domain (Figure 6). In this case the longest $\tau_c$ values are observed for $(x,y,z) \approx (0.577,0.2,0.2)$ (Figure 6b). This vector makes an angle $\alpha = 12°$ with a line that connects the C$\alpha$ of Glu-82 (the first ordered residue of the C-terminal domain) with the center of gravity of the C-terminal domain. Note that small values for the angle $\alpha$ would be expected based on the flexible hinge model, regardless of the average orientation of one domain relative to the other.

*Calculation of the Order Parameters, $S^2$.* For calculating the generalized order parameters, $S^2$ (eq 1), different procedures may be used. Kay et al. (1989) calculated the order parameter exclusively on the basis of the $T_1$ data, using the single $\tau_c$ calculated from averaging all the $\tau_c$ values derived from the $T_1/T_2$ ratios of the individual amides, and assuming that motions on the $\tau_e$ time scale do not contribute to the $^{15}N$ $T_1$ ($\tau_e = 0$ approximation). This procedure was chosen because the $T_1$ data in that case were judged to be more reliable than the $T_2$ or NOE data. As pointed out by Dellwo and Wand (1991), this assumption leads to an overestimate of the actual order parameter in regions of conformational flexibility. However, $S^2$ values based on $T_1$ and NOE data can contain large random errors because the error in the NOE tends to be relatively large. Use of the transverse relaxation ($T_2$) data can also lead to erroneous values since the $T_2$ of a particular $^{15}N$ spin can be shortened dramatically if exchange between conformational substates in the protein makes its chemical shift time-dependent (Kay et al., 1989; Clore et al., 1990a).

As discussed above, the globular domains of calmodulin reorient in a nearly isotropic manner, and we therefore use the isotropic model for the correlation function (eq 2) in deriving the generalized order parameter. Note, however, that the small degree of anisotropy found for the molecular reorientation, discussed in the previous section, causes small errors in the order parameters calculated in this manner; derived order parameters are slightly too low for amides with the N–H bond vector parallel to the axis that has the longest apparent rotational correlation time, and values are a few percent too high for amides oriented perpendicular to this axis.

In the present study, we derive $S^2$ from a combination of the $T_1$, $T_2$, and NOE data, by minimizing the function $f(S^2,\tau_e)$ given by

$$f(S^2,\tau_e) = [(T_{1,\text{calc}} - T_{1,\text{meas}})/T_{1,\text{calc}}]^2 + [(T_{2,\text{calc}} - T_{2,\text{meas}})/T_{2,\text{calc}}]^2 + [(\text{NOE}_{\text{meas}} - \text{NOE}_{\text{calc}})/2]^2 \quad (11)$$

where the subscripts "meas" refers to the measured value. The subscript "calc" refers to the value calculated on the basis of eq 1–3 of Kay et al. (1989), assuming overall correlation times $\tau_c$ of 7.1 and 6.3 ns for the N-terminal domain (residues 3–77) and for the C-terminal domain (residues 78–148), respectively. The importance of the measured NOE, which contains a higher experimental error than the $T_1$ and the $T_2$ data, is scaled down in eq 11 by using a weighting factor of 1/2. For residues that have $T_2$ values shortened by conformational averaging, as identified using eq 7, $S^2$ and $\tau_e$ values are derived on the basis of $T_1$ and NOE data alone, excluding the $T_2$ portion from eq 11.

The calculated order parameters and $\tau_e$ are plotted in Figure 4. As was previously found for staphylococcal nuclease (Kay et al., 1989) and for interleukin-1$\beta$ (Clore et al., 1990a), $S^2$ values are quite uniform in regions of well-defined secondary structure and typically fall in the 0.8–0.9 range. As expected, the N- and C-terminal residues exhibit very low order parameters. More interesting is the high degree of mobility observed near the middle of the central helix, with $S^2 < 0.6$

for residues D78, T79, D80, and S81. Of course, without a high degree of flexibility in this region, the tumbling of the protein would have been highly anisotropic, in contrast with the finding reported above.

In a motional model where the internal motion corresponds to free diffusion in a cone with semiangle, $\alpha$ (Lipari & Szabo, 1982), the order parameter is related to $\alpha$ according to

$$S^2 = [\cos \alpha (1 + \cos \alpha)/2]^2 \quad (12)$$

Thus, for residues D78–S81 the angle $\alpha$ is ~35°. Because there are four consecutive residues for which the amide N–H bond vector experiences internal motions of this magnitude, and because these internal motions must be largely uncorrelated considering the absence of hydrogen bonding (Spera et al., 1991; Ikura et al., 1991b) or other interactions that stabilize their relative orientations, it may be concluded that residues D78–S81 form a quite flexible hinge.

A low order parameter is also observed in the loop region that connects helices B and C, and the homologous loop connecting helices F and G. A recent hydrogen exchange study of calmodulin (Spera et al., 1991) finds the highest hydrogen exchange rates for exactly the same residues for which a low $S^2$ value is found in the present study, with only three exceptions. First, the hydrogen exchange at the C-terminal residue is much slower than anticipated on the basis of its low $S^2$ value ($S^2$ = 0.3). However, it is well-known that base-catalyzed hydrogen exchange of the amide proton of a C-terminal residue is strongly reduced by the presence of negative charge of the nearby carboxy terminus. The other two exceptions occur for residues A57 and I130. Hydrogen exchange data indicate relatively slow exchange for these residues, whereas the order parameters calculated in the present study are remarkably low, 0.69 and 0.63, respectively. A57 and I130 are located in highly homologous positions; these residues occupy the second position in the second calcium binding loop of the N- and C-terminal halves of calmodulin. Considering this homology, it is very unlikely that the low order parameter found for these two residues could be attributed to measurement error. However, at present we do not have any structural explanation for these low $S^2$ values. In principle, an increase in the internuclear N–H distance to 1.05 Å would lower the $S^2$ value by about 0.2, since its calculation is based on a fixed distance of 1.01 Å. However, there is no experimental evidence for any anomaly in the N–H bond length for these two residues. Any such anomaly would be expected to cause a drastic change in the $^1J_{NH}$ coupling constant, but values measured for A57 (93.2 Hz) and I130 (93.5 Hz) are very close to the average value found for this coupling constant.

As demonstrated by Clore et al. (1990a,b) for interleukin-1$\beta$ and for several residues in staphylococcal nuclease, the relaxation data obtained for amides in flexible regions of a protein sometimes cannot be fitted in a satisfactory manner by the simple spectral density function of eq 2. However, if the Lipari–Szabo model is extended to account for internal motions on two different time scales, $\tau_f$ and $\tau_s$, satisfactory fitting of the experimental data can be obtained. For calmodulin, all internal motions in the flexible regions are apparently on a faster time scale than what was observed for interleukin-1$\beta$, and adequate fitting of the data in the present case was obtained with the two-parameter spectral density function of eq 1.

## Discussion and Conclusions

Our study finds that the rotational correlation times, $\tau_c$, measured for the individual amides, are nearly independent of the orientation of the N–H bond vector within the molecular axis system. This small degree of anisotropy found for $\tau_c$ is clearly incompatible with the much larger anisotropy predicted for any rigid dumbbell structure (Table I). In principle, lack of anisotropy could be explained by a rigid calmodulin model with a bend in the central helix and the two halves associating to form a stable nearly spherical globular unit. This is clearly not the case for the following reasons: First, such a globular shape is incompatible with the small-angle X-ray scattering data (Seaton et al., 1985; Heidorn & Trewhella, 1988). Second, no NOE interactions between side chains of the two halves are observed for $Ca^{2+}$-ligated calmodulin (Ikura et al., 1991b). Third, the average $\tau_c$ values calculated for the N-terminal and C-terminal halves (7.12 ± 0.42 ns and 6.30 ± 0.48 ns) differ by almost two standard deviations, suggesting that the two halves reorient at different rates. The probability, $p$, that this difference in $\tau_c$ would arise by chance (i.e., by random measurement error) is essentially zero ($p = 10^{-14}$). Finally, for a nonspherical rigid protein, the apparent rotational correlation time (as obtained from the $T_1/T_2$ ratio) increases relative to a spherical protein of the same volume. In contrast, the $\tau_c$ values measured for calmodulin are significantly shorter than those measured for the nearly spherical proteins staphylococcal nuclease (Kay et al., 1989) and interleukin-1$\beta$ (Clore et al., 1990a), which have approximately the same molecular weight as calmodulin.

The fact that a small degree of motional anisotropy is observed for each of the two domains, with the slowest tumbling perpendicular to axes that connect the middle of the central helix to the center of gravity of its domain, qualitatively supports a "flexible hinge" model. In such a model, the middle of the central helix has a flexible structure, much like a dumbbell with a flexible joint at its center. Reorientation of the individual spheres of the dumbbell in such a case is not quite isotropic and is most rapid about the axis that connects the center of each sphere with the flexible joint. The presence of such a flexible hinge near the middle of the central helix is confirmed by low order parameters, $S^2$, derived from our NMR data for the backbone amides near the middle of the central helix.

Proteolysis experiments indicate that $Ca^{2+}$-saturated calmodulin is sensitive to cleavage near the middle of the central

Table I: Elements of the Rotational Diffusion Tensor (Units of $10^7$ $s^{-1}$) at 35 °C for the Hydrodynamic Models Discussed in the Appendix[a]

| | I[b] | II[c] | IV[d] | V[e] | sphere[f] |
|---|---|---|---|---|---|
| $D_{xx}$ | 1.72 | 1.83 | 1.22 | 1.63 | 3.05 |
| $D_{yy}$ | 1.78 | 1.90 | 1.27 | 1.63 | 3.05 |
| $D_{zz}$ | 4.49 | 4.79 | 2.67 | 4.08 | 3.05 |
| $D_\parallel/D_\perp$ | 2.56 | 2.65 | 2.15 | 2.50 | 1.00 |
| $(2D_\perp + 4D_\parallel)^{-1}$ | 4.66 | 4.37 | 7.59 | 5.11 | 5.46 |
| $(5D_\perp + D_\parallel)^{-1}$ | 7.53 | 7.12 | 11.23 | 8.21 | 5.46 |
| $(6D_\perp)^{-1}$ | 9.51 | 8.90 | 13.42 | 10.29 | 5.46 |
| $T_{1,\parallel}$ | 607 | 576 | 813 | 647 | 417 |
| $T_{2,\parallel}$ | 86 | 91 | 63 | 80 | 135 |
| $\tau_{c,\parallel}$ | 9.51 | 8.88 | 13.36 | 10.26 | 5.46 |
| $T_{1,\perp}$ | 427 | 415 | 564 | 446 | 409 |
| $T_{2,\perp}$ | 127 | 134 | 90 | 119 | 129 |
| $\tau_{c,\perp}$ | 5.79 | 5.44 | 8.85 | 6.27 | 5.46 |

[a] Also included are the decay constants (in ns) for $\langle P_2(\mu(t)\mu(0))\rangle$ in the symmetric top approximation [$D_\perp = D_{xx} + D_{yy})/2$; $D_\parallel = D_{zz}$] and the calculated $T_{1,\perp}$, $T_{1,\parallel}$, $T_{2,\perp}$, and $T_{2,\parallel}$ (in ms), assuming an order parameter ($S^2$) of 0.85. The correlation times $\tau_{c,\perp}$ and $\tau_{c,\parallel}$ obtained from the $T_1/T_2$ ratios. The subscripts "$\parallel$" and "$\perp$" refer to the orientation of the N–H bond vector relative to the unique axis. Note that $T_{1,\parallel}$ is determined by $D_\perp$, etc. [b] All heavy atoms ($\sigma$ = 1.0 Å). [c] Cα carbons only ($\sigma$ = 3.5 Å). [d] Cα carbons ($\sigma$ = 3.5 Å) with 1/2 shell waters ($\sigma$ = 1.6 Å). [e] Dumbbell model with three spheres of 8 beads each. [f] Sphere with a 3-Å hydration layer ($\sigma$ = 19.75 Å).

helix (Drabikowski et al., 1977; Mackall & Klee, 1991), also indicating substantial flexibility in this region of the protein. Previous NMR work also suggested flexibility in the calmodulin central helix. For a review, see Evans et al. (1988). Mutation studies show that, even with the deletion of several residues in the central helix, the protein can maintain near-native binding affinity to its target proteins, even though binding requires both halves of calmodulin to interact simultaneously with the target (Persechini & Kretsinger, 1988; Persechini et al., 1989). This information was interpreted to confirm the "flexible tether" model, where the central helix has a high degree of flexibility and allows calmodulin to bind to a variety of targets.

A number of other experiments have been interpreted to provide support for a rigid dumbbell calmodulin solution structure, however. Seaton et al. (1985) used small-angle X-ray scattering (SAXS) to measure a maximum vector length of 62 Å for $Ca^{2+}$-ligated calmodulin, "consistent with the solution structure of the protein being the same as that of the crystal". More recently, Heidorn and Trewhella (1988) also used SAXS to compare the solution and crystal structures of calmodulin. However, they conclude that, although their maximum vector length of 63 ± 2 Å in itself may not be inconsistent with the crystal structure, the shape of the measured pairwise distance distribution function, $P(r)$, is not compatible with a solution structure identical to the crystal structure. The $P(r)$ function is compatible with a model where the central helix of the crystal structure has a 65° bend near the middle, but also with a situation "where the distance between the globular domains could vary over a large range of values and the solution scattering data reflect the average conformation". A molecular dynamics simulation study (Mehler et al., 1991) supports the latter possibility.

Small and Anderson (1988) conducted dynamic fluorescence anisotropy measurements on covalently modified calmodulin and concluded that $Ca^{2+}$-ligated calmodulin is elongated and has a length equal or nearly equal to that predicted by X-ray crystallographic results. Their conclusion is based primarily on a reorientational correlation time, $\tau_c$ of 9 ns, measured at 20 °C. After correction for the difference in temperature and viscosity, the correlation times measured in our present study are in excellent agreement with the Small and Anderson result. Small and Anderson argue, however, that this correlation time is significantly longer than what would be expected for a hydrated spherical protein of 17.6 kDa using the Stokes–Einstein equation (Cantor & Schimmel, 1980). We do not believe the measured correlation time to be unusually long. In contrast, as pointed out earlier, the correlation time measured for CaM is shorter than what is found for nearly spherical globular proteins of similar size, using the same NMR approach. Small and Anderson explained the lack of nonexponentiality in the anisotropy decay observed in their experiments by calculating the diffusion tensor elements for a rigid dumbbell. However, as discussed in the Appendix, this conclusion was based on an older bead model that severely underestimates motional anisotropy.

The present $^{15}N$ relaxation study unequivocally indicates a very high degree of mobility for residues 78–81 in the central helix. This mobility is responsible for the fact that, from an $^{15}N$ relaxation view point, the N- and C-terminal halves reorient nearly isotropically. The motional correlation times for the two halves are slightly different and compatible with the difference in size of their structured regions.

Our NMR study shows that (a) the correlation times for the two domains differ proportionally to their size, (b) the correlation times derived for the individual amides depend only weakly on the orientation of the N–H bond vector, to a much lesser degree than predicted by hydrodynamic calculations for rigid dumbbell models, (c) the correlation times are shorter than observed for other globular proteins of similar mass, and (d) the order parameters for the amides near the middle of the central helix are low. These findings strongly support the "flexible tether" hypothesis, where the central helix only serves to keep the two domains in close proximity for binding to their target.

## Acknowledgments

We thank Claude B. Klee for continous help, encouragement, and stimulating discussions, Marie Krinks for preparing the calmodulin sample used in this study, Richard Venable for assistance with the hydrodynamic calculations, Attila Szabo, Dennis Torchia, Marius Clore, and Robert Powers for useful discussions, and Giulia Donadel for her caring assistance during the preparation of the manuscript. The calmodulin coding construct was kindly provided to us by Kathy Beckingham and John F. Maune.

## Appendix

*Hydrodynamic Calculations for Rigid Calmodulin Models.* This appendix calculates the degree of anisotropy expected for "rigid" calmodulin, and the effect of such anisotropic tumbling on the NMR parameters $T_1$ and $T_2$.

The elements of the rotational diffusion tensor are estimated using the bead model approximation, with the calmodulin crystal structure (Babu et al., 1988) as a reference. In this approximation, a polymer is modeled as a collection of point sources of friction (denoted beads) with hydrodynamic interactions described by the Oseen tensor or modified Oseen tensor (Garcia de la Torre & Bloomfield, 1981). The translational and rotational friction tensors for the array of $N$ beads are then calculated from the solution of a set of linear equations or, operationally, by numerically inverting a $3N \times 3N$ matrix (Garcia de la Torre & Bloomfield, 1981). This is readily accomplished on a scientific workstation for systems of $N$ up to 500–1000. The bead sizes depend both on the application and on computer limitations. For large proteins and viruses the beads are on the order of a protein or protein domain (Garcia de la Torre & Bloomfield, 1977, 1981); small to intermediate size proteins and small molecules can also be modeled with the beads representing individual atoms (Pastor & Karplus, 1988; Venable & Pastor, 1988). This latter approach allows a more detailed description of the irregular surfaces of polymers than is possible with simple surfaces such as spheres, ellipsoids, and cylinders, at the cost of increased computational time.

Given the uncertainties of applying hydrodynamic models to proteins, the sensitivity of the ratio $D_\parallel/D_\perp$ is explored using four different bead models, from detailed to simple: (I) all heavy atoms; (II) $\alpha$-carbons only; (III) C$\alpha$ carbons with 1/2 shell waters; (IV) a dumbbell model with three spheres of 8 beads each. These models are described in more detail below.

(*I*) *All Heavy Atoms* ($\sigma$ = *1* Å). In this model each heavy atom is represented by a bead of radius $\sigma$. This model was used earlier to calculate diffusion constants for pancreatic trypsin inhibitor, lysozyme, and ribonuclease (Venable & Pastor, 1988). Because of the relatively large number of beads for calmodulin (1134), the diffusion constants are relatively insensitive to the precise value of the bead radius and the value $\sigma$ = 1.0 Å was used here. Diffusion constants are then calculated in a manner described by Garcia de la Torre and Bloomfield (1981).

*(II) α-Carbons Only* ($\sigma$ = *3.5* Å). Diffusion constants that are approximately the same as for model I can be obtained by representing the Cα nuclei of the protein by beads of $\sigma$ = 3.5 Å. This reduces the number of beads to 142 for calmodulin (no coordinates are available for the first five residues and for the last one), greatly decreasing the computer time for calculating the diffusion tensor.

*(III) α-Carbons* ($\sigma$ = *3.5* Å) *with 1/2 Shell of Waters* ($\sigma$ = *1.6* Å). When beads of atomic dimensions are used for hydrodynamic modeling of proteins, a partial layer of water is required to obtain quantitative agreement with experimental translational and rotational diffusion constants (Teller et al., 1979; Venable & Pastor, 1988). Therefore, models I and II are expected to overestimate $D_\parallel$ and $D_\perp$, although their ratio may still be fairly accurate. A grid placement procedure (Venable & Pastor, 1988) was used to add 364 waters (represented by beads of $\sigma$ = 1.6 Å) to the surface of calmodulin; 364 waters correspond to approximately 1/2 shell. For computational efficiency only the Cα carbons were retained, resulting in a total of 506 beads. From earlier work, a half shell is the approximate upper limit for the number of hydrodynamically bound waters (Venable & Pastor, 1988).

*(IV) Dumbbell Model with Three Spheres Consisting of 8 Beads Each.* Here, calmodulin is modeled by three colinear spheres: two large ones (radius $\sigma_1$) for the globular domains and a smaller one (radius $\sigma_2$) for the spacer (central helix). The length of the spacer is $L$, so when the three spheres are touching, $L = 2\sigma_2$. Following Small and Anderson (1988) we assume a hydrated volume of 25 200 Å$^3$ and $\sigma_2$ = 3.5 Å, which then makes $\sigma_1$ = 14.2 Å and gives a total length ($4\sigma_1 + 2\sigma_2$) of 63.8 Å, in reasonable agreement with the crystal structure. Each of the three spheres of the dumbbell was modeled by a cubic array of 8 beads (with suitably adjusted radii) (Garcia Bernal & Garcia de la Torre, 1981), rather than by a single bead used in the Small and Anderson study. As pointed out by Garcia de la Torre and Bloomfield (1981), their earlier dumbbell modeling studies (1977), in which each of the spheres of the dumbbell is represented by a single bead, yield relatively inaccurate results for $D_\perp$ when $L/\sigma_1 < 5$; i.e., the two spheres must be well separated. For calmodulin, $L/\sigma_1 \approx 1/2$, and the calculations of Small and Anderson, based on the earlier Garcia de la Torre and Bloomfield (1977) model, resulted in a significant overestimate of $D_\perp$ and a corresponding underestimate of $D_\parallel/D_\perp$.

The results for all four models are shown in Table I. They are calculated for a temperature of 35 °C, and $\eta$ = 0.7194 (the viscosity of pure water at this temperature); to scale the results to 20 °C, multiply the diffusion constants by 0.6845. Table I indicates that the diffusion anisotropy ($D_\parallel/D_\perp$) shows little variation for models I–IV. As expected, the magnitudes of the diffusion tensor elements decrease with increasing hydration. Also given in Table I are the diffusion constants and relaxation times that would be expected if calmodulin were spherical, assuming a partial specific volume of 0.707 cm$^3$/g (Crouch & Klee, 1980) and a 3-Å hydration shell, resulting in a radius of 19.75 Å. The rotational correlation time of a sphere with volume $V$ in a medium of viscosity $\eta$ is given by the well-known expression:

$$\tau_c = \eta V/kT \qquad \text{(A1)}$$

where $k$ is Boltzmann's constant and $T$ is the absolute temperature. Use of a 3-Å hydration layer is necessary to bring the calculated and observed rotational correlation times for proteins into close agreement (Venable & Pastor, 1988). Note that for the nearly spherical proteins staphylococcal nuclease and interleukin-1β, which have volumes nearly identical to that of calmodulin, rotational correlation times of ~8 ns were obtained from $^{15}$N relaxation studies (Kay et al., 1989; Clore et al., 1990a), suggesting that 3 Å is a low estimate for the size of the hydration layer, or that $\tau_c$ values measured by $^{15}$N NMR tend to be longer than theory predicts.

Table I also shows the apparent rotational correlation times (which would be obtained from the $T_1/T_2$ ratio in the standard manner) that would be obtained for N–H bond vectors perpendicular ($\tau_{c,\perp}$) and parallel ($\tau_{c,\parallel}$) to the long axis of the molecule. Clearly, anisotropy of motion increases both the apparent $\tau_{c,\parallel}$ and $\tau_{c,\perp}$ (albeit to a lesser degree) compared to a spherical molecule of the same volume. Therefore, rotational correlation times significantly longer than 8 ns would be expected if the solution structure of calmodulin were a rigid dumbbell, particularly for amides with the N–H bond vector oriented parallel to the long axis of the protein.

## Supplementary Material Available

One table reporting the observed $T_1$, $T_2$, and NOE values for 114 residues in calmodulin, together with the rotational correlation time, $\tau_c$, the order parameter, $S^2$, and the correlation time for internal motion, $\tau_e$, derived for these residues, and six figures, showing enlargements of Figures 5a–c and 6a–c with labeling of the individual residues and their apparent correlation times (11 pages). Ordering information is given on any current masthead page.

## References


Babu, Y. S., Bugg, C. E., & Cook, W. J. (1988) *J. Mol. Biol. 204*, 191–204.

Boyd, J., Hummel, U., & Campbell, I. D. (1990) *FEBS Lett. 175*, 477–482.

Cantor, C. R., & Schimmel, P. R. (1980) *Biophysical Chemistry*, p 461, Freeman, San Francisco.

Clore, G. M., Driscoll, P. C., Wingfield, P. T., & Gronenborn, A. M. (1990a) *Biochemistry 29*, 7387–7401.

Clore, G. M., Szabo, A., Bax, A., Kay, L. E., Driscoll, P. C., & Gronenborn, A. M. (1990b) *J. Am. Chem. Soc. 112*, 4989–4991.

Cohen, P., & Klee, C. B., Eds. (1988) *Calmodulin*, Elsevier, New York.

Dellwo, M. J., & Wand, A. J. (1991) *J. Magn. Reson. 91*, 505–516.

Drabikowski, W., Kuznicki, J., & Grabarek, Z. (1977) *Biochim. Biophys. Acta 485*, 124–133.

Evans, J. S., Levine, B. A., Williams, R. J. P., & Wormald, M. R. (1988) *Calmodulin* (Cohen, P., & Klee, C. B. Eds.) pp 57–82, Elsevier, New York.

Garcia Bernal, J., & Garcia de la Torre, J. (1981) *Biopolymers 20*, 129–139.

Garcia de la Torre, J., & Bloomfield, V. A. (1977) *Biopolymers 16*, 1765–1778.

Garcia de la Torre, J., & Bloomfield, V. A. (1981) *Q. Rev. Biophys. 14*, 81–139.

Heidorn, D. B., & Trewhella, J. (1988) *Biochemistry 27*, 909–915.

Hubbard, P. S. (1970) *J. Chem. Phys. 52*, 563–568.

Huntress, W. T. (1968) *J. Chem. Phys. 48*, 3524–3533.

Ikura, M., Kay, L. E., & Bax, A. (1990a) *Biochemistry 29*, 4659–4667.

Ikura, M., Marion, D., Kay, L. E., Shih, H., Krinks, M., Klee, C. B., & Bax, A. (1990b) *Biochem. Pharmacol. 40*, 153–160.

Ikura, M., Kay, L. E., Krinks, M., & Bax, A. (1991a) *Biochemistry 30*, 5498–5504.

Ikura, M., Spera, S., Barbato, G., Kay, L. E., Krinks, M., &

Bax, A. (1991b) *Biochemistry 30*, 9216-9228.
Kay, L. E., Torchia, D. A., & Bax, A. (1989) *Biochemistry 28*, 8972-8979.
Kay, L. E., Nicholson, L. K., Delaglio, F., Bax, A., & Torchia, D. A. (1992) *J. Magn. Reson. 97*, 359-375.
Kretsinger, R. H., Rudnick, S. E., & Weissman, L. J. (1986) *J. Inorg. Biochem. 28*, 289-302.
Lipari, G., & Szabo, A. (1982) *J. Am. Chem. Soc. 104*, 4546-4558.
Mackall, J., & Klee, C. B. (1991) *Biochemistry 30*, 7242-7247.
Matsushima, N., Izumi, Y., Matsuo, T., Yoshino, H., Ueki, T., & Miyake, Y. (1989) *J. Biochem. (Tokyo) 105*, 883-887.
Mehler, E. L., Pascual-Ahuir, J.-L., & Weinstein, H. (1991) *Protein Eng. 4*, 625-637.
Messerle, B. A., Wider, G., Otting, G., Weber, C., & Wuthrich, K. (1989) *J. Magn. Reson. 85*, 608-613.
Nirmala, N. R., & Wagner, G. (1988) *J. Am. Chem. Soc. 110*, 7557-7559.
Palmer, A. G., Skelton, N. J., Chazin, W. J., Wright, P. E., & Rance, M. (1992) *Mol. Phys. 75*, 699-711.
Pastor, R. W., & Karplus, M. (1988) *J. Phys. Chem. 92*, 2636-2641.
Persechini, A., & Kretsinger, R. (1988) *J. Biol. Chem. 263*, 12175-12178.
Persechini, A., Blumenthal, D. K., Jarrett, H. W., Klee, C. B., Hardy, D. O., & Kretsinger, R. H. (1989) *J. Biol. Chem. 264*, 8052-8058.
Seaton, B. A., Head, J. F., Engelman, D. M., & Richards, F. M. (1985) *Biochemistry 24*, 6740-6743.
Shatzman, A. R., & Rosenberg, M. (1985) *Ann. N.Y. Acad. Sci. 478*, 233-248.
Sklenar, V., Torchia, D. A., & Bax, A. (1987) *J. Magn. Reson. 73*, 375-379.
Small, E., & Anderson, S. R. (1988) *Biochemistry 27*, 419-428.
Spera, S., Ikura, M., & Bax, A. (1991) *J. Biomol. NMR 1*, 155-165.
Taylor, D. A., Sack, J. S., Maune, J. F., Beckingham, K., & Quiocho, F. A. (1991) *J. Biol. Chem. 266*, 21375-21380.
Teller, D. C., Swanson, E., & de Haen, C. (1979) *Methods Enzymol. 61*, 103-124.
Venable, R. M., & Pastor, R. W. (1988) *Biopolymers 27*, 1001-1014.
Walsh, M., Stevens, F. C., Kuznicki, J., & Drabikowski, W. (1977) *J. Biol. Chem. 252*, 7740-7743.
Woessner, D. T. (1962) *J. Chem. Phys. 37*, 647-654.

# Increased Thermal Stability of Proteins in the Presence of Naturally Occurring Osmolytes†

Marcelo M. Santoro, Yufeng Liu, Saber M. A. Khan, Li-Xiang Hou, and D. W. Bolen*
*Department of Chemistry and Biochemistry and Department of Medical Biochemistry, Southern Illinois University, Carbondale, Illinois 62901-4409*

*Received December 28, 1991; Revised Manuscript Received March 24, 1992*

ABSTRACT: Organisms and cellular systems which have adapted to stresses such as high temperature, desiccation, and urea-concentrating environments have responded by concentrating particular organic solutes known as osmolytes. These osmolytes are believed to confer protection to enzyme and other macromolecular systems against such denaturing stresses. Differential scanning calorimetric (DSC) experiments were performed on ribonuclease A and hen egg white lysozyme in the presence of varying concentrations of the osmolytes glycine, sarcosine, *N*,*N*-dimethylglycine, and betaine. Solutions containing up to several molar concentrations of these solutes were found to result in considerable increases in the thermal unfolding transition temperature ($T_m$) for these proteins. DSC scans of ribonuclease A in the presence of up to 8.2 M sarcosine resulted in reversible two-state unfolding transitions with $T_m$ increases of up to 22 °C and unfolding enthalpy changes which were independent of $T_m$. On the basis of the thermodynamic parameters observed, 8.2 M sarcosine results in a stabilization free energy increase of 7.2 kcal/mol for ribonuclease A at 65 °C. This translates into more than a 45 000-fold increase in stability of the native form of ribonuclease A over that in the absence of sarcosine at this temperature. Catalytic activity measurements in the presence of 4 M sarcosine give $k_{cat}$ and $K_m$ values that are largely unchanged from those in the absence of sarcosine. DSC of lysozyme unfolding in the presence of these osmolytes also results in $T_m$ increases of up to 23 °C; however, significant irreversibly occurs with this protein. Naturally occurring glycine-based osmolytes appear to provide a general method of stabilizing proteins against thermal unfolding even well beyond the physiological concentration range for osmolyte, and the degree of stabilization can be extraordinary.

Considerable time in nearly all fields of biochemical sciences is devoted to stabilizing proteins and developing empirical formulations and protocols for retaining the activity of purified preparations of peptides and proteins. While protein stabilization is a vexing issue in research, it is no less of a problem in living systems (Yancey et al., 1982). Organisms have constantly had to address the problem, and have done so with far more constraints and fewer options than are faced in a laboratory setting. In particular, organisms which are subjected to environmental stresses such as heat, dehydration, or extreme solution conditions such as high salt or urea must maintain biological activity in the face of rather severe denaturing stresses (Somero & Clark, 1985; Somero, 1986;

† Supported by a grant from Biotechnology Research Development Corp.
* Address correspondence to this author at the Department of Chemistry and Biochemistry, Southern Illinois University.

0006-2960/92/0431-5278$03.00/0 